Special Issue

Optical Coherence Tomography Based Estimates of Crystalline Lens Volume, Equatorial Diameter, and Plane Position

Eduardo Martinez-Enriquez, Mengchan Sun, Miriam Velasco-Ocana, Judith Birkenfeld, Pablo Pérez-Merino, and Susana Marcos

Instituto de Óptica Daza de Valdés, Consejo Superior de Investigaciones Científicas (CSIC), C/Serrano, 121, 28006, Madrid, Spain

Correspondence: Eduardo Martinez-Enriquez, Instituto de Óptica Daza de Valdés, Consejo Superior de Investigaciones Científicas, C/ Serrano, 121, 28006 Madrid, Spain; eduardo.martinez@io.cfmac.csic.es.

Submitted: December 14, 2015
Accepted: July 23, 2016

Citation: Martinez-Enriquez E, Sun M, Velasco-Ocana M, Birkenfeld J, Pérez-Merino P, Marcos S. Optical coherence tomography based estimates of crystalline lens volume, equatorial diameter, and plane position. *Invest Ophthalmol Vis Sci*. 2016;57:OCT600–OCT610. DOI:10.1167/iovs.15-18933

Purpose. Measurement of crystalline lens geometry in vivo is critical to optimize performance of state-of-the-art cataract surgery. We used custom-developed quantitative anterior segment optical coherence tomography (OCT) and developed dedicated algorithms to estimate lens volume (VOL), equatorial diameter (DIA), and equatorial plane position (EPP).

Methods. The method was validated ex vivo in 27 human donor (19–71 years of age) lenses, which were imaged in three-dimensions by OCT. In vivo conditions were simulated assuming that only the information within a given pupil size (PS) was available. A parametric model was used to estimate the whole lens shape from PS-limited data. The accuracy of the estimated lens VOL, DIA, and EPP was evaluated by comparing estimates from the whole lens data and PS-limited data ex vivo. The method was demonstrated in vivo using 2 young eyes during accommodation and 2 cataract eyes.

Results. Crystalline lens VOL was estimated within 96% accuracy (average estimation error across lenses ± standard deviation: 9.30 ± 7.49 mm^3). Average estimation errors in EPP were below 40 ± 32 μm, and below 0.26 ± 0.22 mm in DIA. Changes in lens VOL with accommodation were not statistically significant (2-way ANOVA, $P = 0.35$). In young eyes, DIA decreased and EPP increased statistically significantly with accommodation ($P < 0.001$) by 0.14 mm and 0.13 mm, respectively, on average across subjects. In cataract eyes, VOL = 205.5 mm^3, DIA = 9.57 mm, and EPP = 2.15 mm on average.

Conclusions. Quantitative OCT with dedicated image processing algorithms allows estimation of human crystalline lens volume, diameter, and equatorial lens position, as validated from ex vivo measurements, where entire lens images are available.

Keywords: cataract surgery, lens, optical coherence tomography

Understanding the properties of the crystalline lens of the human eye is crucial for the design and evaluation of solutions for presbyopia and for cataracts.

Human crystalline lens geometry has been widely studied ex vivo[1–10] and in vivo.[11–28] In vivo measurements of the crystalline lens typically come from Purkinje,[22–24] Scheimpflug,[12–15,18,19,24] magnetic resonance imaging,[11,17,26,28] and optical coherence tomography (OCT).[16,25,27] To obtain accurate anterior and posterior lens shape estimates, optical imaging methods must be corrected from optical distortion produced by refraction by the cornea and anterior lens surfaces.[18,29] In addition, optical imaging in the eye only allows the retrieval of information visible through the pupil, preventing direct calculation of some important parameters such as the equatorial plane position (EPP), the volume (VOL), or the diameter of the lens at the equatorial plane (DIA).

Accurate estimation of the EPP is very useful to predict where an intraocular lens (IOL) will be placed after cataract surgery (estimated lens position [ELP]) and, thus, of great value in the selection of the IOL power to be implanted in a patient. Current IOL power selection is normally based on limited preoperative input data[30] (typically axial length and corneal power[31,32] and, in some cases, lens thickness[33,34]) and statistical regression formulae obtained from a large population.[30,35–39] In previous reports we demonstrated the accurate construction of OCT-based patient-specific computer eye models.[40,41] Selection of an IOL based on ray tracing computation on patient-specific eye models, together with a more accurate estimation of the ELP will undoubtedly result in better refractive, optical and visual outcomes.[42]

Preoperative estimations of crystalline lens VOL will be of high value in emerging treatments of presbyopia. In particular, knowledge of lens VOL is critical in lens refilling techniques, in which the degree of filling of the capsular bag is essential to achieve the appropriate refraction and an adequate amplitude of accommodation.[43–45] It is also fundamental in the selection of several accommodative IOLs (A-IOLs), where prior knowledge of the DIA and VOL could enhance refractive predictability and be critical for the correct mechanism of action of the A-IOL.[46,47] Finally, estimation of the shape of the entire lens can be useful to be used in patient-dependent mathematical models and finite element modeling of the eye.[48–50]

A scarce number of studies have reported in vivo the shape of the entire lens and associated interesting parameters EPP, VOL, or DIA. Most of these reports are based on magnetic resonance imaging[11,17,26,28] of the lens, which is able to

capture nondistorted images of the entire lens, although with significantly lower resolutions and much higher acquisition times than optical techniques. Previous approaches to estimate lens VOL, EPP, and DIA from optical techniques do not attempt to model the equatorial region of the lenses, but rather estimate those parameters from the intersection of the two parametric surfaces that best fit the data within the pupil (available data) of the anterior lens (AL) and the posterior lens (PL) surfaces[13,43] (Hwang K-Y, et al. *IOVS* 2015;56: ARVO E-Abstract 1356). This method, which will be referred throughout the paper as the intersection approach, results in an overestimation of VOL and DIA and underestimation (anterior shift) of EPP. Other methods consider a constant value for the EPP[48] (relative to the lens thickness), although some reports suggest that EPP is subject-dependent.[26]

Optical coherence tomography provided with fan and optical distortion correction algorithms[29,51] has shown to be an excellent technique to image the anterior segment of the eye, due to its high resolution and high speed.[52–56] In this study, the shape of the entire lens and, therefore, VOL, DIA, and EPP were estimated from in vivo OCT measurements. The method was validated using 27 ex vivo lenses (in which the information of the whole lens was available). In vivo conditions were simulated for three-dimensional (3D) OCT volumes, assuming that only the information within a given pupil size (PS) was available. The entire lens geometry was estimated from the limited pupil information using a parametric model, and the lens VOL, DIA, and EPP compared to those computed from the whole lens. Finally, these models were applied to in vivo measurements in 2 young eyes during accommodation and 2 cataract eyes.

Materials and Methods

Human Lens

Donor Eyes. Thirty-five eyes from 30 human donors (between 19 and 71 years of age), obtained from Transplant Service Foundation Eye Bank were used in the experiments. Results from this set of eyes (gradient refractive index [GRIN], thickness, curvature radius, and topography) were reported previously.[3,57,58] Eyes were shipped in sealed vials at 4°C and wrapped in gauze soaked in preservation medium (Dulbecco modified Eagle medium/F-12 medium [DMEM/F-12], HEPES, no phenol red; Gibco, Carlsbad, CA, USA). The lens was carefully extracted from the eye and immersed in the same preservation medium at room temperature. During the measurements, the lens was placed horizontally on a ring in a DMEM-filled cuvette. Damage, incomplete (not whole lens information available), or excessively tilted lenses were identified from OCT images and excluded from the study, therefore leaving 27 useful lenses (9 lenses <45 and 18 lenses >45 years of age). The handling and experimental protocols had been previously approved by the Institutional Review Boards of Transplant Service Foundation and CSIC. Methods for securing human tissue were in compliance with the Declaration of Helsinki.

In-Vivo Measurements. Two eyes from 2 young subjects (33 and 32 years of age; spherical errors 0 D and −1.5 D and cylinder <0.25 D) were measured during accommodation (relaxed and 6 D stimulation). Two eyes from cataract patients (65 and 70 years of age; spherical errors −1.5 D and −2 D and cylinder <1.25 D) were measured prior to cataract surgery. Subjects signed a consent form approved by the Institutional Review Boards after they had been informed of the nature and possible consequences of the study, in accordance with the tenets of the Declaration of Helsinki.

OCT Imaging

The OCT images were acquired using a custom-developed spectral OCT system previously described.[59] Briefly, the set up was based on a fiberoptic Michelson interferometer configuration with a superluminescent diode ($\lambda_0 = 840$ nm; $\Delta\lambda = 50$ nm) as a light source and a spectrometer consisting of a volume diffraction grating and a complementary metal-oxide semiconductor camera as a detector. The effective acquisition speed was 25,000 A-scan/s. The axial range was 7 mm in depth in air, resulting in a theoretical pixel resolution of 3.4 μm. The nominal axial resolution was 6.9 μm in tissue.

For donor eyes, one 3D volume was composed of 1168 A-scans, and 60 B-scans on a 12 × 12 mm lateral area, acquired in 4.5 seconds. The lens was first completely imaged with the anterior surface facing the OCT beam and then flipped around a predetermined axis and imaged again with the posterior surface up. More details can be found in Birkenfeld et al.[58]

For accommodation measurements, one 3D volume was composed of 300 A-scans, and 50 B-scans on a 11 × 11 mm lateral area, acquired in 0.6 second, showing a good balance between time acquisition and resolution. A Badal system mounted on a motorized stage (VXM-1; Velmex, Bloomfield, NY, USA) was used for compensating defocus and for inducing accommodation. Five repeated measurements were collected in each accommodation state (0 D and 6 D) after inducing mydriasis with 1 drop of phenylephrine. More details are described in Perez-Merino et al.[27] For cataract measurements, one 3D volume was composed of 360 A-scans and 50 B-scans on a 7 × 15 mm lateral area, acquired in 0.72 second. Five repeated measurements were taken under natural conditions for relaxed accommodation. More details can be found in Marcos et al.[60] The specifications of the spectrometer and light source did not allowed sufficient axial range to capture all anterior segment surfaces in a single acquisition. To solve that, three sets of 3D images were captured sequentially at 5 seconds after blinking: (1) cornea, (2) anterior lens, and (3) posterior lens, shifting axially the plane of focus; all 3D sets of data contained the iris.

OCT Image Processing

Ex Vivo Human Lens. The full volume of the lens was obtained by segmenting the first surface imaged under each condition[61] (anterior surface in "anterior-up" images, posterior surface in "posterior-up" images) and then registering both anterior and posterior surfaces. B-scans were processed with semiautomatic surface segmentation algorithms and fan and optical distortion correction algorithms (group refractive index of the solution was taken as 1.345 at 825 nm).[62] Registration was achieved by identifying, for both AL and PL, the lens cross-section parallel to *x-y* plane (i.e., normal to the optical axis of the lens, *z*) exhibiting maximum area (i.e., the equatorial plane, where curvature changes from AL to PL) and by finding the 3D displacement that maximized the intersection area between both (AL and PL) cross-sectional planes. Figure 1 shows raw OCT images ("anterior-up" [left] and "posterior-up" [middle] measurements) and reconstructed volumes (right) for 38-year-old (Fig. 1A) and 67-year-old (Fig. 1B) donor lenses.

In Vivo Human Lens. Corneal and lens surfaces were automatically segmented for every B-scan, using previously described custom-designed algorithms.[27,63] Three-dimensional segmented corneal, AL, and PL surfaces were registered using the pupil center (obtained from the automatically identified iris volume in every of the three captured images in different depths) as a reference.[27] Registered volumes were corrected for fan and optical distortion using 3D ray tracing routines.[29,51] The corneal group refractive index was taken as 1.385,[64] the

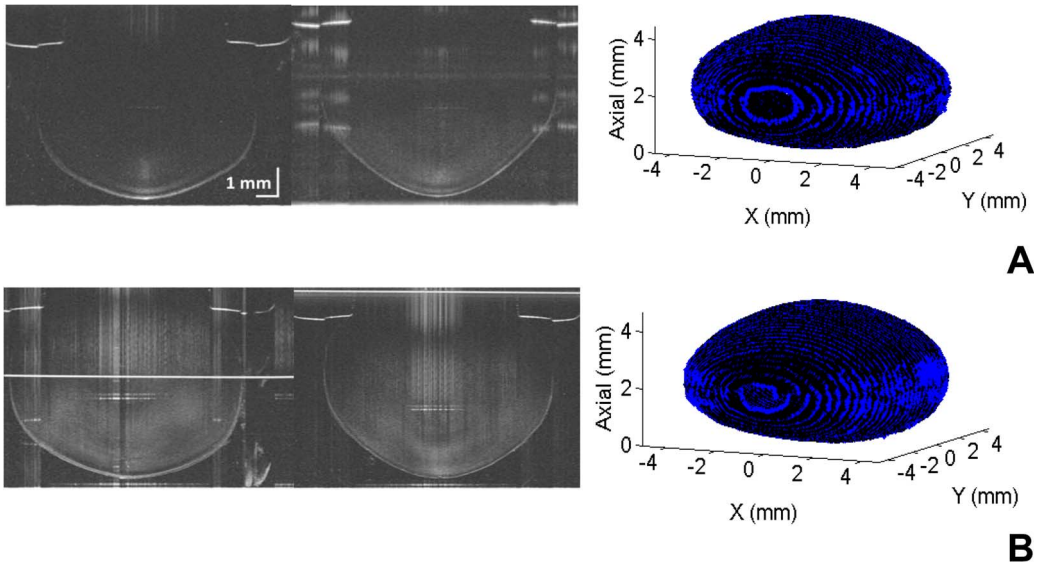

FIGURE 1. Raw OCT images of "anterior-up" (*left*) and "posterior-up" (*middle*) measurements and reconstructed volumes (*right*). (**A**) A 38-year-old lens; (**B**) a 67-year-old lens.

aqueous humor group refractive index as 1.345, and the crystalline lens refractive index was obtained from the age dependent average group refractive index expression derived by Uhlhorn et al.[10]

Lens Shape Estimation

Lens Model Construction. From the ex vivo full lens volume (Fig. 2A, black points), we assumed that only data within a specific PS were available (Fig. 2A, green points), simulating in vivo conditions. From these PS data, the construction of 3D models of the entire lens included the following steps:

Step 1: Fitting of AL and PL surfaces within PS to parametric models (Fig. 2B), obeying the following equation[65]:

$$z_{con} = \frac{\theta_1(x-x_0)^2 + \theta_2(y-y_0)^2}{1+\sqrt{1-(1+\theta_3)\theta_1^2(x-x_0)^2-(1+\theta_4)\theta_2^2(y-y_0)^2}} + z_0, \quad (1)$$

where x and y are the coordinates of the sampling points within PS (i.e., so that $x^2 + y^2 \leq (PS/2)^2$); and vector $\theta = (\theta_1,\theta_2,\theta_3,\theta_4,x_0,y_0,z_0)$ contains the parameters of the surface. Note that $\theta_1 = 1/R_x$, $\theta_2 = 1/R_y$, $\theta_3 = Q_x$ and $\theta_4 = Q_y$ in biconicoids; $\theta_1 = \theta_2 = 1/R$ and $\theta_3 = \theta_4 = Q$ in conicoids; and $\theta_1 = c/a^2$, $\theta_2 = c/b^2$, $\theta_3 = a^2/c^2 - 1$, and $\theta_4 = b^2/c^2 - 1$ in ellipsoids, with a, b, and c the semi-axes of the ellipsoid along x, y, and z (axial) axes. Terms (x_0,y_0,z_0) are the coordinates of the center of the parametric surface. The fitting was performed using a nonlinear multidimensional minimization algorithm.

Step 2: Extrapolation of the nonavailable central portion of the lens. Data within α (diameter that defines the central portion, with $\alpha \geq PS$) were extrapolated in AL and PL using the best fitted parametric surfaces (θ^*) from Equation 1 in the domain defined by α:

$$z_{ext} = z_{con}(\theta^*, x, y), \quad (2)$$

with $x^2 + y^2 \leq (\alpha/2)^2$, as illustrated in Fig. 2C.

Step 3: Estimation of the equatorial region of the lens, fitting four parametric surfaces (lens sides) to the extrapolated AL and PL data in Equation 2. Specifically, a part ρ of the central portion (z_{ext}) measured inward starting from an outermost end of z_{ext} was taken to fit every lens side, that is, lens side 1: $\forall\, x, y \leq -\alpha/2 + \rho$; lens side 2: $x \geq \alpha/2 - \rho$, $\forall\, y$; lens side 3: $\forall\, x, y \geq \alpha/2 - \rho$; and lens side 4: $x \leq -\alpha/2 + \rho$, $\forall\, y$.

The fitting was performed using Equation 1, interchanging the coordinate z with x (lens sides 2 and 4) or y (lens sides 1 and 3) in order to obtain a surface oriented along the desired axis.[65] Figure 2D shows the data taken (blue points) to fit the lens side 1 (Fig. 2E, green surface). Figure 2F shows the final lens model after the fitting of the four surfaces (lens side 1 in green, lens side 2 in pink, lens side 3 in orange, and lens side 4 in yellow).

Parameters Training. The reconstructed lens shape depends on the chosen α and ρ values (i.e., large α values will lead to an overestimation of DIA and VOL and vice-versa; large ρ will lead to smoother lens equatorial regions but lower ability of the model to adapt to fast curvature changes). The optimal α depends on the lens geometry, in particular, lens DIA. As DIA is not known a priori, α is chosen as a proportion (PROP) of the diameter in the intersection (ID) of the anterior and posterior fitting surfaces from Equation 1, which can be calculated for every lens (i.e., $\alpha = PROP * ID$). Figure 3 shows the definition of ID, equatorial plane position (EPP), which is given as the distance from AL apex, and other parameters of interest.

The training process consisted on finding (using cross-validation) the parameters PROP and ρ which minimized the following function:

$$J(PROP,\rho) = \mathrm{VOLe}(PROP,\rho) + \mathrm{DIAe}(PROP,\rho) + \mathrm{EPPe}(PROP,\rho), \quad (3)$$

where VOLe, DIAe, and EPPe are the mean estimation errors (absolute value of the difference between the estimation and the actual value) across lenses, normalized by subtracting their means and dividing by their standard deviations to be comparable.

Data Analysis

The estimated VOL, DIA, and EPP from PS-limited data in ex vivo lenses were compared for different PS values with those obtained using the entire lens. The estimation errors from the

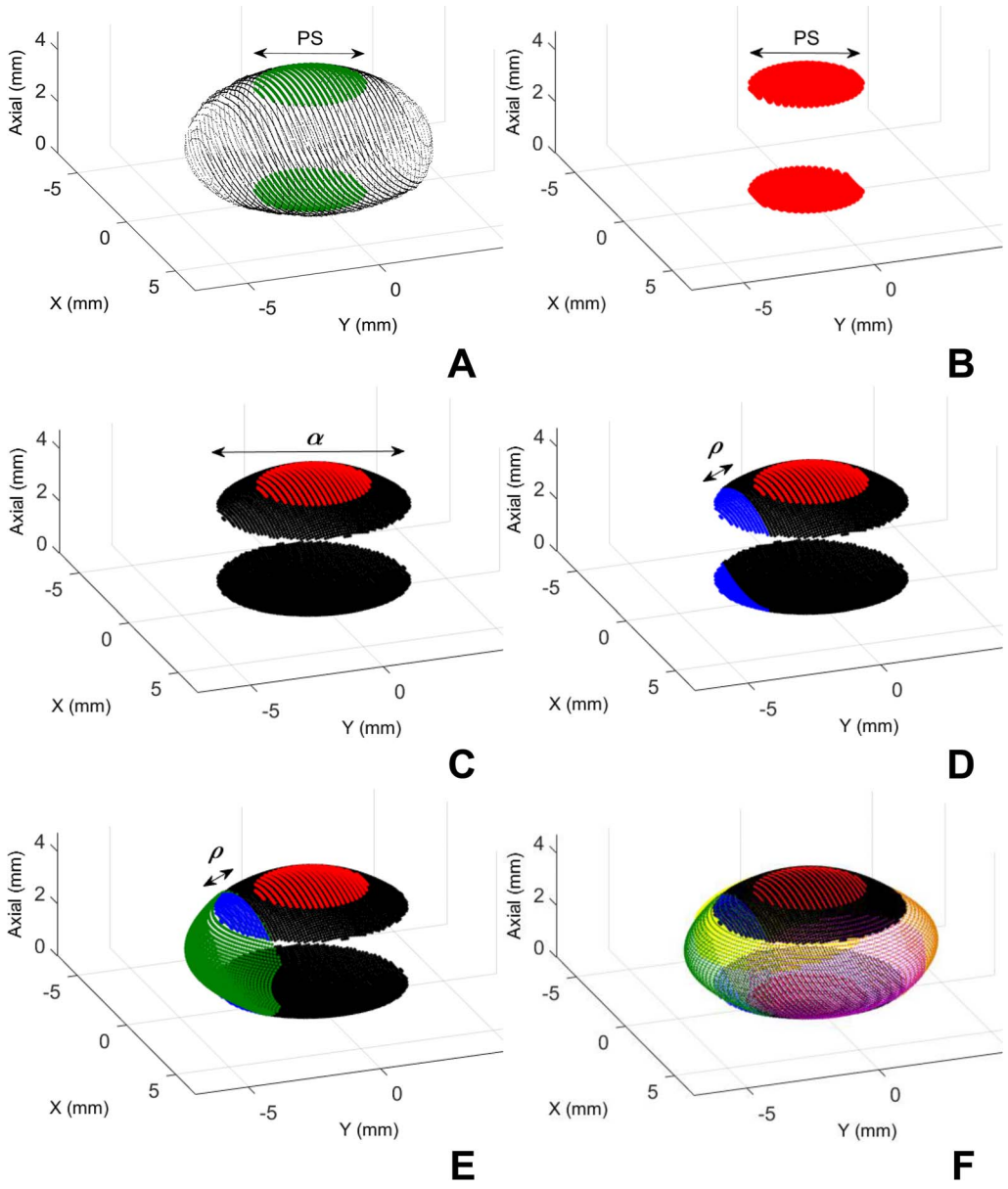

FIGURE 2. Lens construction process. (**A**) Ex vivo full lens volume and PS. (**B**) Fitting of AL and PL surfaces within PS to parametric models. (**C**) Extrapolation of the nonavailable central part of the lens. (**D, E**) Estimation of one side of the equatorial region of the lens. (**F**) Final estimated lens.

proposed method were compared with those obtained from other methods in previous reports. VOL, DIA, and EPP are estimated from 2 young eyes (relaxed and accommodated) and 2 cataract eyes. Statistical analysis (2-way ANOVA) was conducted to study significant dependences of the VOL, DIA, and EPP with accommodation, subject, and interaction.

RESULTS

Evaluation of the Performance of the Estimation Model

Evaluation of Lens Shape Fitting Surfaces. Ellipsoids, conicoids and biconicoids were evaluated in Equation 1 for the fitting of the central and equatorial regions of the lens. The VOL, DIA, and EPP estimation errors were approximately the same using ellipsoids and biconicoids, and were higher with conicoids. Given the similar performance of ellipsoids and biconicoids, ellipsoids were chosen to fit the central as well as the equatorial regions of the lens because they needed a lower number of parameters to be optimized, preventing overfitting.

Evaluation of the Estimation Error as a Function of the Model Parameters. Figure 4A shows the error surface *J(PROP, ρ)* (Equation 3) and the optimal parameters found in the training process, $PROP^*$ and ρ^*. Also, we studied the VOL (Fig. 4B), DIA (Fig. 4C), and EPP (Fig. 4D) average estimation error (with sign) as a function of (PROP,ρ) pairs. For any ρ, as PROP tends to 1, the model approximates to an intersection approach (Fig. 3, purple points). When PROP and ρ are low, the VOL and DIA are underestimated and the EPP is overestimated.

Estimation Error Results. The errors in the estimation of VOL, DIA, and EPP were calculated using the optimal $PROP^*$ and ρ^* parameters. Figure 5, blue bars, shows the error in the

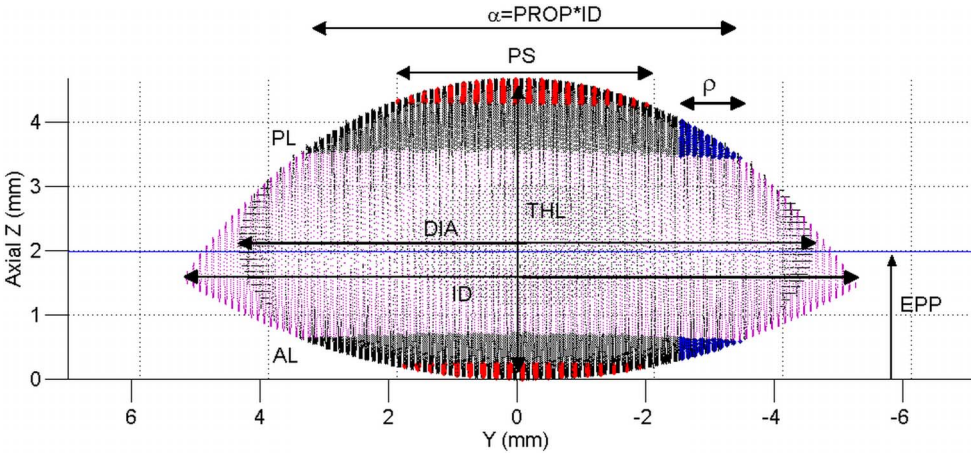

Figure 3. Lens model and definition of some parameters of interest. α, diameter that defines the central portion of the lens; AL, anterior lens; DIA, diameter; EPP, equatorial plane position; ID, diameter in the intersection; PL, posterior lens; PROP, proportion of the diameter in the intersection; PS, pupil size; ρ, part of the central portion taken to fit every lens side.

estimation of VOL (Fig. 5A), DIA (Fig. 5B), and EPP (Fig. 5C) for each individual lens, using PS = 5 mm, with the proposed method. Volume, DIA, and EPP estimation errors were below 20 mm^3, 0.9 mm, and 100 μm, respectively, for all lenses. On average (Fig. 6, blue bars), crystalline lens VOL (Fig. 6A) was estimated within 96% accuracy (mean errors across lenses: 9.30 ± 7.49, 8.29 ± 7.00, and 6.92 ± 6.43 mm^3 for PS = 4, 4.5 and 5 mm, respectively). Errors in DIA (Fig. 6B) were 0.26 ± 0.22, 0.24 ± 0.23, and 0.22 ± 0.21 mm, respectively, and EPP (Fig. 6C) was estimated with error <45 μm (errors of 40 ± 32, 39 ± 34, and 36 ± 32 μm, respectively).

Comparison With Other Approaches

Figure 5 compares the estimated VOL (Fig. 5A), DIA (Fig. 5B), and EPP (Fig. 5C) with the proposed method and state-of-the-art approaches for each individual ex vivo lens for PS = 5 mm. Volume and DIA estimation errors were compared with the intersection approach[2,12,43] (Hwang K-Y, et al. *IOVS* 2015;56: ARVO E-Abstract 1356) and EPP with the constant value (EPP/thickness = 0.41) proposed by Rosen et al.[2] VOL, DIA, and EPP estimation errors with the state-of-the-art approaches were below 42 mm^3, 2 mm, and 300 μm, respectively, for all the lenses. Figure 6 shows the average VOL (Fig. 6A) and DIA (Fig.

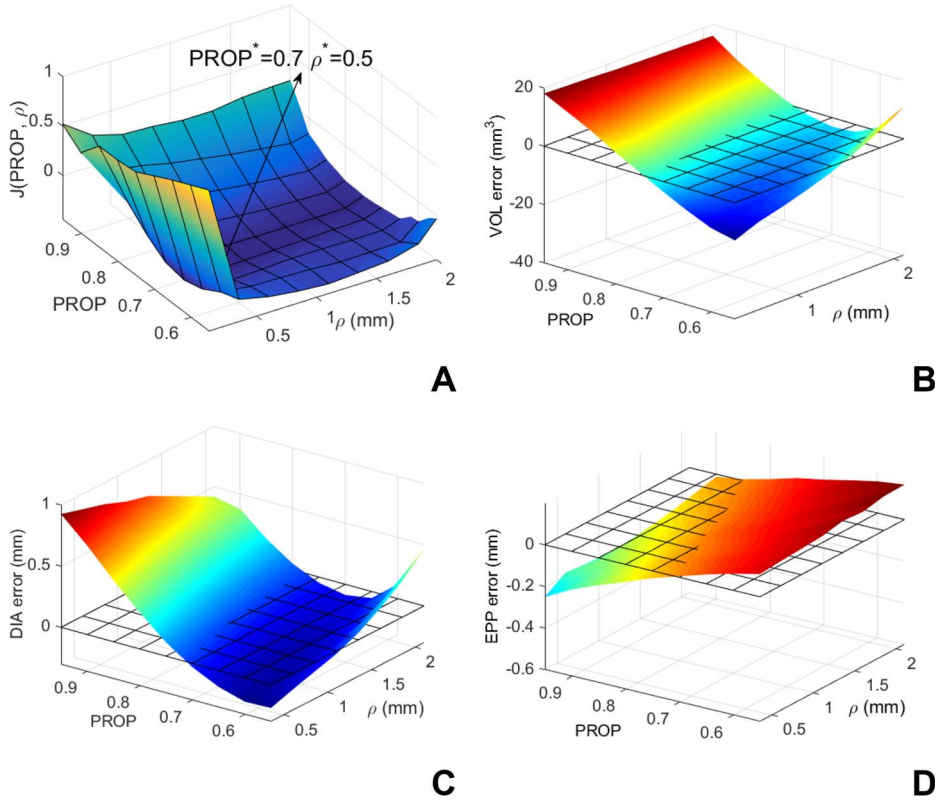

Figure 4. (**A**) *J(PROP, ρ)* as a function of PROP and ρ, and optimal PROP* and ρ* found. (**B–D**) VOL (**B**), DIA (**C**), and EPP (**D**) estimation error (with sign) as a function of ρ and PROP.

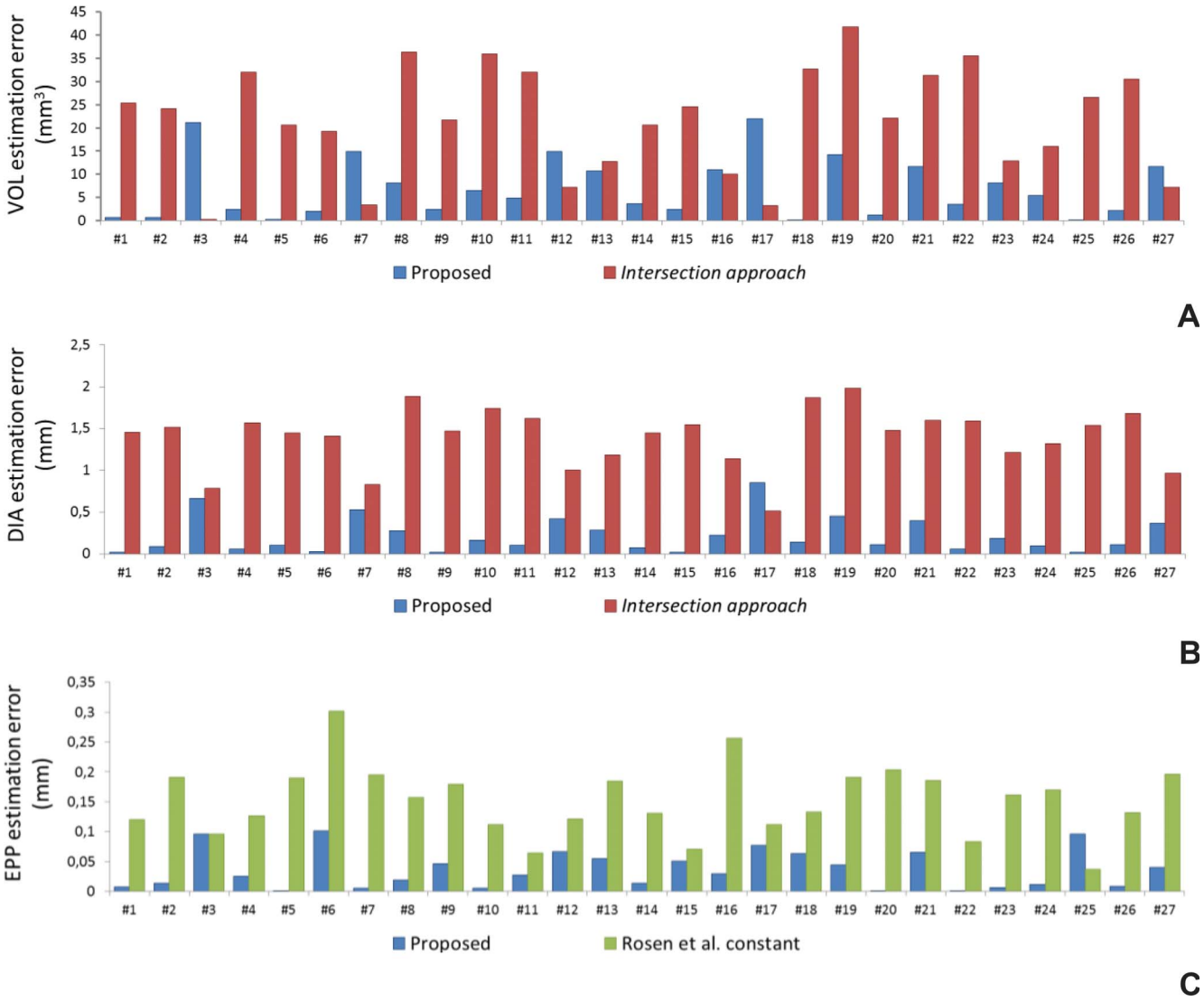

Figure 5. Estimation error of the proposed and state-of-the-art approaches for each individual lens, PS = 5 mm. (**A**) VOL estimation error (cubic millimeters). (**B**) Diameter estimation error (millimeters). (**C**) EPP estimation error (millimeters).

6B) estimation errors across lenses with the proposed method and the intersection approach. Figure 6C shows the average EPP estimation error with the proposed method and with other methods applied: (1) intersection approach, (2) a constant value derived from our data set (EPP/thickness = 0.43), (3) the constant value from Rosen et al.,[2] and (4) with EPP = thickness/2. Estimates for PS = 4, 4.5 and 5 mm are shown.

Changes of the In Vivo Crystalline Lens Shape With Accommodation

Volume, DIA, and EPP were estimated in 2 young subjects in vivo during accommodation (for 0 D and 6 D, PS = 5 mm). Differences in lens VOL with accommodation were not statistically significant (2-way ANOVA, $P = 0.35$), with average values across measurements of 179.8 ± 3.5 (0 D) and 180.3 ± 2.8 (6 D) mm³ in S1 and of 155.2 ± 3.3 and 155.4 ± 3.3 mm³ in S2. Diameter decreased with accommodation (statistically significant, 2-way ANOVA, $P < 0.001$) from 9.46 ± 0.05 to 9.32 ± 0.06 mm in S1 and from 8.58 ± 0.07 to 8.44 ± 0.06 mm in S2, and EPP increased, that is, backward shifted (statistically significant, 2-way ANOVA, $P < 0.001$) from 1.72 ± 0.02 to 1.82 ± 0.02 mm in S1 and from 2.02 ± 0.02 to 2.19 ± 0.03 mm in S2. Note that subject had also significant effects in DIA, EPP, and VOL and that the interaction was significant in EPP. Figure 7 shows raw OCT volumes (Fig. 7, left) and anterior segment reconstruction, including the estimation of the whole crystalline lens (Fig. 7, right), for S1 in 0 D (Fig. 7A) and 6 D (Fig. 7B).

Crystalline Lens VOL, DIA, and EPP in Cataract Eyes

In the cataract eyes, the estimated average values across measurements (PS = 4 mm) were VOL = 198.3 ± 3.8 and 213.4 ± 3.6 mm³, DIA = 9.46 ± 0.05 and 9.68 ± 0.07 mm, and EPP = 2.07 ± 0.02 and 2.23 ± 0.03 mm in both subjects, respectively. Figure 8 shows raw OCT volumes (Fig. 8, left), anterior segment reconstruction, and estimation of the whole crystalline lens (Fig. 8, right) for S1.

Discussion

In this study we proposed a method to estimate in vivo the VOL, DIA, and EPP from OCT distortion-corrected images.

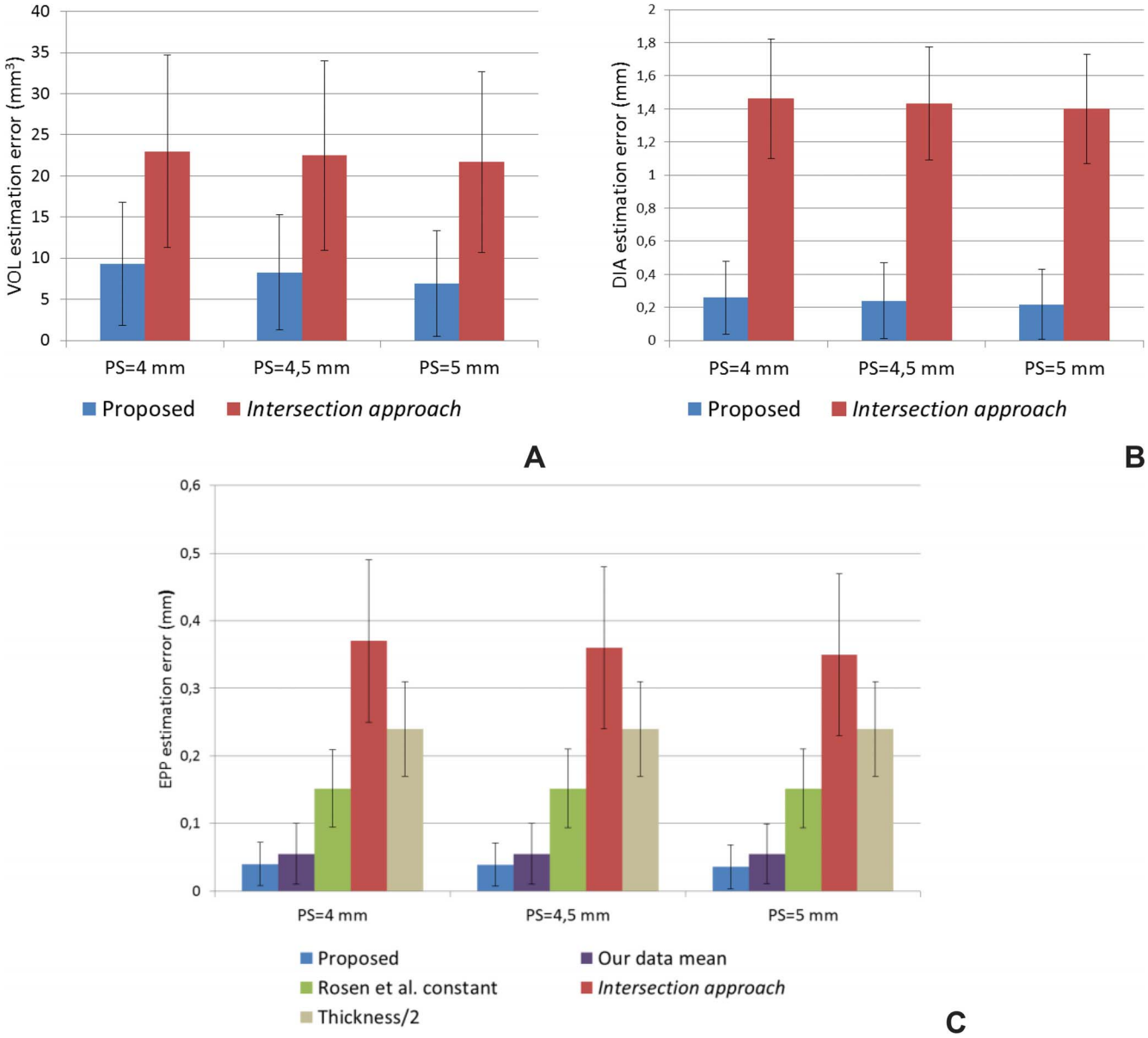

FIGURE 6. (**A**) Average VOL estimation error (cubic millimeters) of the proposed and the intersection approach. (**B**) Average DIA estimation error (millimeters) of the proposed and the intersection approach. (**C**) Average EPP estimation error (millimeters) of the proposed method, using the Rosen et al.[2] constant, thickness/2, our data mean, and the intersection approach. Data are for PS = 4, 4.5, and 5 mm.

Estimation models were constructed from ex vivo measurements assuming that only the information within the pupil was available. As images of the entire lens were available, we could validate the accuracy of the method by comparing the nominal lens parameters to those reconstructed from data limited by the pupil. Finally, lens VOL, DIA, and EPP were estimated in vivo in both accommodating eyes and cataract eyes using these models.

Comparison With Earlier Work

The proposed method showed an improved performance in comparison with state-of-the-art methods, leading to VOL, DIA, and EPP estimation errors approximately 3, 6, and 4 times lower on average, respectively (Fig. 6).

In the accommodating eyes, we found that VOL remained constant with accommodation, DIA decreased and EPP shifted backwards, which is consistent with previously reported results by Hermans et al.,[26] and Marussich et al.[9] However, Gerometta et al.[66] measured an increase of lens VOL with accommodation.

Sources of Error

The main source of error in the construction of lens volumes ex vivo comes from the merging process, which may lead to errors in the calculation of the actual VOL, DIA, and EPP of the whole ex vivo lenses, and therefore incorrect estimation errors (VOLe, DIAe, and EPPe) in Equation 3, and discrepancies in the calculation of the optimal parameters ρ and PROP. We simulated the effect of merging errors on the estimated VOL, DIA, and EPP, by assuming a Gaussian variability in posterior lens axial shifts ($\mu = 0$ and $\sigma = 0.25$ mm, which is likely higher than real shifts). With these variations, optimal PROP changed

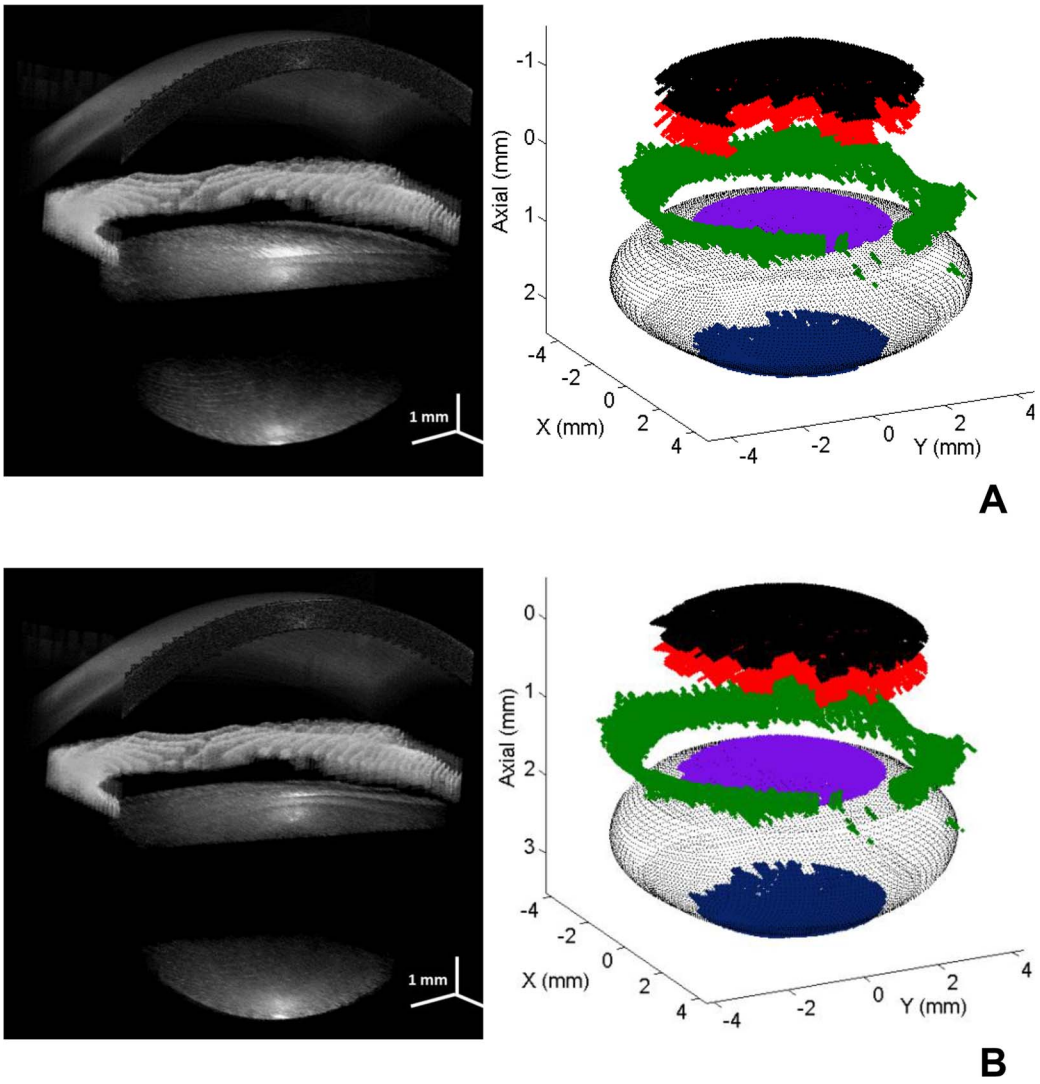

FIGURE 7. Raw OCT volumes (*left*), anterior segment reconstruction and estimated lens (*right*) for S1. (**A**) 0 D. (**B**) 6 D.

from 0.7 to 0.75 and ρ from 0.5 to 1.5, leading to average estimation errors of 7.23 ± 5.69 mm^3 in VOL, 0.12 ± 0.09 in DIA, and 42 ± 33 μm in EPP, showing that merging errors are not critical for the performance of the algorithm.

Sources of error in in vivo measurements have been analyzed in previous studies.[27] We estimated experimentally that the effect of the OCT lateral sampling, axial resolution and merging process produced errors of <1% in VOL, DIA, and EPP.

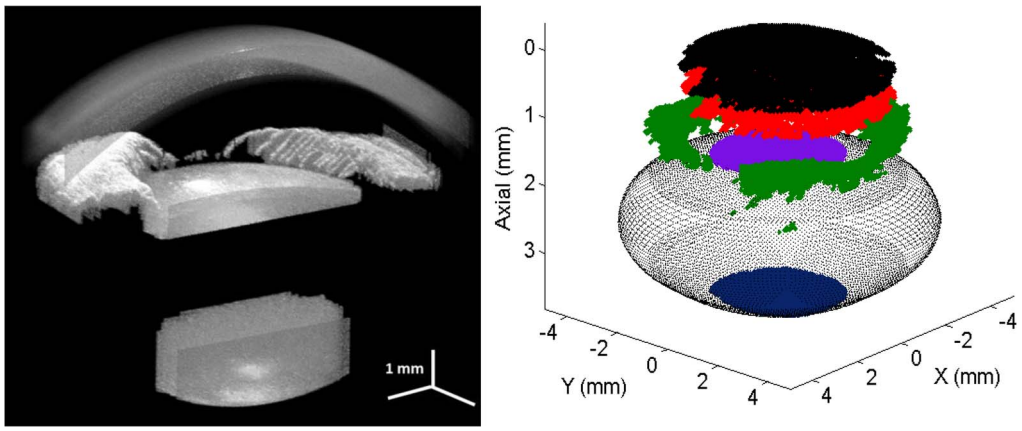

FIGURE 8. Raw OCT volumes (*left*), anterior segment reconstruction and estimated lens (*right*) for S1.

The horizontal ex vivo orientation, opposed to the up-right orientation of the lens in vivo, may create some changes associated to the influence of gravity. Some works have reported that gravity has a small effect on crystalline lens parameters, as spherical aberration or lens thickness,[5,67] suggesting that gravity will likely have a negligible impact on our results.

Distortion Correction

Fan and optical distortions corrections are crucial to obtain accurate quantitative data and therefore accurate estimations of the entirely lens shape (VOL, DIA, EPP). As noted in previous publication,[27] if distortions are not corrected, anterior lens and posterior lens curvature radii will be highly overestimated. We compared lens parameter estimates with and without fan and optical distortion corrections in lenses in vivo and found that not correcting for these distortions resulted in an overestimation of VOL by 25%, of DIA by 15%, and an anterior shift of EPP by 8%.

Advantages of 3D Imaging

Besides differences in the imaging modality and the lens parametric modeling, most previous studies are based on cross-sectional images of the lens.

We evaluated the benefits of using 3D imaging compared to 2D cross-sectional images. For every whole 3D lens image, 8 different evenly spaced (pi/8) 2D meridians through the lens center were taken, simulating 8 different measurements acquired with 2D imaging techniques. For every meridian, a 3D rotationally symmetric model was constructed, and the VOL, DIA, and EPP estimation errors using these rotationally symmetric models and the models from the OCT 3D imaging were compared. The simulation was performed using 1000 randomly chosen 2D meridians of each lens. On average (across meridians and lenses), the mean VOL estimation error increased from 9.30 mm^3 to 12.28 mm^3, the DIA from 0.26 mm to 0.34 mm, and the EPP from 40 μm to 61 μm, when using 2D versus 3D data sets. These errors will be larger for 2D meridians that differed from the average profile (VOL, DIA, and EPP estimation errors up to 20.31 mm^3, 0.55 mm, and 133 μm, respectively) or when the 2D measurement is not obtained through the lens apex. These results are in agreement with recent studies that reveal the relevance of lens surface astigmatism[3,27] and errors associated to the assumption of lens rotational symmetry.[9] The proposed approach could be implemented in current commercial devices such as Scheimpflug-imaging based systems or clinical anterior segment OCT. Nevertheless, as demonstrated before, distortion correction is critical to obtain accurate results.[18,29,68]

Influence of GRIN

The ex vivo lens volumes were constructed from two sets of OCT measurements obtained with the anterior lens surface up and posterior surface up, not affected by the GRIN. However, in vivo OCT measurements of the posterior lens surface were obtained through the anterior surface, assuming a homogeneous refractive index in the optical distortion correction. Marussich et al.[9] showed that an uncertainty of ±0.01 in the refractive index produced an uncertainty on the order of ±1% in the lens VOL and suggested that ignoring the GRIN introduced a negligible error. Siedlecki et al.[69] showed that GRIN did not affect significantly the estimation of lens radii of curvature, although posterior lens asphericity estimates may in fact be affected by neglecting the presence of GRIN. Recent estimates of GRIN distribution profiles in human lenses[57,58] can be used to further refine the estimates.

Extrapolation of Ex Vivo-Based Lens Model to In Vivo Applications

Lens models have been trained with isolated ex vivo lenses with a wide range of geometries. A large number of our lens sample correspond to nearly presbyopic or presbyopic eyes, where one expects minimal changes with accommodation and thus ex vivo and in vivo lenses are expected to have approximately the same shape. In addition, the fact that we did not find a dependency on the optimal parameters ($PROP^*$ and ρ^*) across lenses of different ages and that VOL was estimated to be constant with accommodation in vivo, suggests that the method can also be applied in vivo in young lenses. The model could be further refined using a sample with younger lenses mounted in a stretcher system.[9]

Implications for IOL Power Selection

Preoperative estimation of postoperative IOL position is the largest contribution of refractive outcome errors (35%).[42] Therefore, improvements in the prediction of postoperative IOL position will be critical to achieve a better IOL selection.

As previously reported by Hermans et al.,[26] we also found that the EPP/thickness changed across individuals (from 0.40 to 0.47 in our data set; from 0.39 to 0.46 in the study by Hermans et al.[26]), indicating the limitation of assuming a constant value and stressing the importance of individual anatomical measurements for proper estimation of the ELP. For example, using Rosen et al's constant,[2] EPP/thickness resulted in a mean EPP estimation error of 152 ± 58 μm (Fig. 6) and was close to 300 μm in 2 lenses and approximately 200 μm in 8 lenses (Fig. 5), which would result in a refractive error of approximately 0.5 to 0.6 D in the IOL power calculation in short eyes.[30] Estimations of the EPP by using an intersection approach[2,12,43] (Hwang K-Y, et al. *IOVS* 2015;56: ARVO E-Abstract 1356) or the thickness/2 leads to even higher IOL power errors.

Conversely, the estimation error with the proposed method was below 100 μm in all lenses, suggesting that IOL power selection using the proposed approach to estimate the ELP will further improve previous proposals which included for the first time lens thickness data.[33] Regression equations are generally corrected by the use of an A constant, suggested for each IOL by the manufactured and normally adjusted from clinical outcomes. In some cases the assumption that the IOL position matches the natural equatorial lens position may not hold (i.e., angulated haptics or biomechanical response of the lens). However, knowledge of the lens whole shape, and in particular lens volume, will be very valuable to estimate the deviation of the ELP from the EPP using a systematic approach. Full OCT-based 3D quantification of the anterior segment of the eye and accurate estimation of ELP in patients prior to cataract surgery will pave the way to patient-specific computer eye models and ray tracing based IOL power selection. Further studies on patients before and after cataract surgery will provide further support.

In summary, quantitative OCT with dedicated image processing algorithms allows estimation of human crystalline lens volume, diameter and equatorial lens position, as validated from ex vivo measurements, where entire lens images are available. Patient-specific eye models that include the information on lens volume and equatorial position are critical for better IOL selection (based on ray tracing instead of traditional regression formulas), and will help in presbyopia-correcting

paradigms including crystalline lens refilling and accommodative IOLs.

Acknowledgments

Supported by Ministerio de Educación y Ciencia, Spain, grants FIS2011-25637 and FIS2014-56643, European Research Council grant ERC-2011-AdG-294099 (SM), and Marie Curie ITN grant FP7-PEOPLE-2010-ITN 264605 (MS).

Disclosure: **E. Martinez-Enriquez**, None; **M. Sun**, None; **M. Velasco-Ocana**, None; **J. Birkenfeld**, None; **P. Pérez-Merino**, None; **S. Marcos**, P

References

1. Glasser A, Campbell MC. Biometric, optical and physical changes in the isolated human crystalline lens with age in relation to presbyopia. *Vision Res*. 1999;39:1991–2015.
2. Rosen AM, Denham DB, Fernandez V, et al. In vitro dimensions and curvatures of human lenses. *Vision Res*. 2006;46:1002–1009.
3. Sun M, Birkenfeld J, de Castro A, Ortiz S, Marcos S. OCT 3D surface topography of isolated human crystalline lenses. *Biomed Opt Express*. 2014;5:3547–3561.
4. Borja D, Manns F, Ho A, et al. Optical power of the isolated human crystalline lens. *Invest Ophthalmol Vis Sci*. 2008;49:2541–2548.
5. Glasser A, Campbell MC. Presbyopia and the optical changes in the human crystalline lens with age. *Vision Res*. 1998;38:209–229.
6. Manns F, Fernandez V, Zipper S, et al. Radius of curvature and asphericity of the anterior and posterior surface of human cadaver crystalline lenses. *Exp Eye Res*. 2004;78:39–51.
7. Kim E, Ehrmann K, Uhlhorn S, Borja D, Arrieta-Quintero E, Parel JM. Semiautomated analysis of optical coherence tomography crystalline lens images under simulated accommodation. *J Biomed Opt*. 2011;16:056003.
8. Urs R, Manns F, Ho A, et al. Shape of the isolated ex vivo human crystalline lens. *Vision Res*. 2009;49:74–83.
9. Marussich L, Manns F, Nankivil D, et al. Measurement of crystalline lens volume during accommodation in a lens stretcher. *Invest Ophthalmol Vis Sci*. 2015;56:4239–4248.
10. Uhlhorn SR, Borja D, Manns F, Parel JM. Refractive index measurement of the isolated crystalline lens using optical coherence tomography. *Vision Res*. 2008;48:2732–2738.
11. Atchison DA, Markwell EL, Kasthurirangan S, Pope JM, Smith G, Swann PG. Age-related changes in optical and biometric characteristics of emmetropic eyes. *J Vis*. 2008;8(4):29.
12. Cook CA, Koretz JF, Pfahnl A, Hyun J, Kaufman PL. Aging of the human crystalline lens and anterior segment. *Vision Res*. 1994;34:2945–2954.
13. Koretz JF, Cook CA, Kaufman PL. Aging of the human lens: changes in lens shape at zero-diopter accommodation. *J Opt Soc Am A Opt Image Sci Vis*. 2001;18:265–272.
14. Dubbelman M, Van der Heijde GL, Weeber HA. Change in shape of the aging human crystalline lens with accommodation. *Vision Res*. 2005;45:117–132.
15. Dubbelman M, Van der Heijde GL, Weeber HA, Vrensen GF. Changes in the internal structure of the human crystalline lens with age and accommodation. *Vision Res*. 2003;43:2363–2375.
16. Ortiz S, Perez-Merino P, Gambra E, de Castro A, Marcos S. In vivo human crystalline lens topography. *Biomed Opt Express*. 2012;3:2471–2488.
17. Kasthurirangan S, Markwell EL, Atchison DA, Pope JM. MRI study of the changes in crystalline lens shape with accommodation and aging in humans. *J Vis*. 2011;11(3):19.
18. Dubbelman M, Van der Heijde GL. The shape of the aging human lens: curvature, equivalent refractive index and the lens paradox. *Vision Res*. 2001;41:1867–1877.
19. Dubbelman M, van der Heijde GL, Weeber HA. The thickness of the aging human lens obtained from corrected Scheimpflug images. *Optom Vis Sci*. 2001;78:411–416.
20. Adhi M, Ferrara D, Mullins RF, et al. Characterization of choroidal layers in normal aging eyes using enface swept-source optical coherence tomography. *PLoS One*. 2015;10:e0133080.
21. de Castro A, Rosales P, Marcos S. Tilt and decentration of intraocular lenses in vivo from Purkinje and Scheimpflug imaging. Validation study. *J Cataract Refract Surg*. 2007;33:418–429.
22. Rosales P, Marcos S. Phakometry and lens tilt and decentration using a custom-developed Purkinje imaging apparatus: validation and measurements. *J Opt Soc Am A Opt Image Sci Vis*. 2006;23:509–520.
23. Garner LF, Yap MK. Changes in ocular dimensions and refraction with accommodation. *Ophthalmic Physiol Opt*. 1997;17:12–17.
24. Rosales P, Dubbelman M, Marcos S, van der Heijde R. Crystalline lens radii of curvature from Purkinje and Scheimpflug imaging. *J Vis*. 2006;6(10):5.
25. Gambra E, Ortiz S, Perez-Merino P, Gora M, Wojtkowski M, Marcos S. Static and dynamic crystalline lens accommodation evaluated using quantitative 3-D OCT. *Biomed Opt Express*. 2013;4:1595–1609.
26. Hermans EA, Pouwels PJ, Dubbelman M, Kuijer JP, van der Heijde RG, Heethaar RM. Constant volume of the human lens and decrease in surface area of the capsular bag during accommodation: an MRI and Scheimpflug study. *Invest Ophthalmol Vis Sci*. 2009;50:281–289.
27. Pérez-Merino P, Velasco-Ocana M, Martinez-Enriquez E, Marcos S. OCT-based crystalline lens topography in accommodating eyes. *Biomed Opt Express*. 2015;6:5039–5054.
28. Sheppard AL, Evans CJ, Singh KD, Wolffsohn JS, Dunne MC, Davies LN. Three-dimensional magnetic resonance imaging of the phakic crystalline lens during accommodation. *Invest Ophthalmol Vis Sci*. 2011;52:3689–3697.
29. Ortiz S, Siedlecki D, Grulkowski I, et al. Optical distortion correction in optical coherence tomography for quantitative ocular anterior segment by three-dimensional imaging. *Opt Express*. 2010;18:2782–2796.
30. Olsen T. Calculation of intraocular lens power: a review. *Acta Ophthalmol Scand* 2007;85:472–485.
31. Sanders DR, Kraff MC. Improvement of intraocular lens power calculation using empirical data. *J Am Intraocul Implant Soc*. 1980;6:263–267.
32. Sanders DR, Retzlaff JA, Kraff MC, Gimbel HV, Raanan MG. Comparison of the SRK/T formula and other theoretical and regression formulas. *J Cataract Refract Surg*. 1990;16:341–346.
33. Olsen T, Corydon L, Gimbel H. Intraocular lens power calculation with an improved anterior chamber depth prediction algorithm. *J Cataract Refract Surg*. 1995;21:313–319.
34. Norrby S. Using the lens haptic plane concept and thick-lens ray tracing to calculate intraocular lens power. *J Cataract Refract Surg*. 2004;30:1000–1005.
35. Olsen T, Hoffmann P. C constant: new concept for ray tracing-assisted intraocular lens power calculation. *J Cataract Refract Surg*. 2014;40:764–773.
36. Preussner PR, Olsen T, Hoffmann P, Findl O. Intraocular lens calculation accuracy limits in normal eyes. *J Cataract Refract Surg*. 2008;34:802–808.

Investigative Ophthalmology & Visual Science

37. Preussner PR, Wahl J, Weitzel D, Berthold S, Kriechbaum K, Findl O. Predicting postoperative intraocular lens position and refraction. *J Cataract Refract Surg*. 2004;30:2077–2083.
38. Olsen T. Prediction of the effective postoperative (intraocular lens) anterior chamber depth. *J Cataract Refract Surg*. 2006; 32:419–424.
39. Olsen T, Funding M. Ray-tracing analysis of intraocular lens power in situ. *J Cataract Refract Surg*. 2012;38:641–647.
40. Ortiz S, Perez-Merino P, Duran S, et al. Full OCT anterior segment biometry: an application in cataract surgery. *Biomed Opt Express*. 2013;4:387–396.
41. Sun M, Pérez-Merino P, Martinez-Enriquez E, Velasco-Ocana M, Marcos S. Full 3-D OCT-based pseudophakic custom computer eye model. *Biomed Opt Express*. 2016;7:1074–1088.
42. Norrby S. Sources of error in intraocular lens power calculation. *J Cataract Refract Surg*. 2008;34:368–376.
43. Nishi O, Nishi Y, Chang S, Nishi K. Accommodation amplitudes after an accommodating intraocular lens refilling procedure: in vivo update. *J Cataract Refract Surg*. 2014;40: 295–305.
44. Koopmans SA, Terwee T, Glasser A, et al. Accommodative lens refilling in rhesus monkeys. *Invest Ophthalmol Vis Sci*. 2006; 47:2976–2984.
45. Nishi Y, Mireskandari K, Khaw P, Findl O. Lens refilling to restore accommodation. *J Cataract Refract Surg*. 2009;35: 374–382.
46. Pepose JS. Design strategies for new accommodating IOLs. *J Cataract Refract Surg*. January 2009. Available at: http:// crstoday.com/2009/01/CRST0109_07.php/.
47. McLeod SD, Vargas LG, Portney V, Ting A. Synchrony dual-optic accommodating intraocular lens. Part 1: optical and biomechanical principles and design considerations. *J Cataract Refract Surg*. 2007;33:37–46.
48. Hermans EA, Dubbelman M, van der Heijde GL, Heethaar RM. Estimating the external force acting on the human eye lens during accommodation by finite element modelling. *Vision Res*. 2006;46:3642–3650.
49. Smith G, Atchison DA, Iskander DR, Jones CE, Pope JM. Mathematical models for describing the shape of the in vitro unstretched human crystalline lens. *Vision Res*. 2009;49: 2442–2452.
50. Weeber HA, van der Heijde RG. Internal deformation of the human crystalline lens during accommodation. *Acta Ophthalmol*. 2008;86:642–647.
51. Ortiz S, Siedlecki D, Remon L, Marcos S. Optical coherence tomography for quantitative surface topography. *Appl Opt*. 2009;48:6708–6715.
52. Dunne MC, Davies LN, Wolffsohn JS. Accuracy of cornea and lens biometry using anterior segment optical coherence tomography. *J Biomed Opt*. 2007;12:064023.
53. Gora M, Karnowski K, Szkulmowski M, et al. Ultra high-speed swept source OCT imaging of the anterior segment of human eye at 200 kHz with adjustable imaging range. *Opt Express*. 2009;17:14880–14894.
54. Huang D, Swanson EA, Lin CP, et al. Optical coherence tomography. *Science*. 1991;254:1178–1181.
55. Shen M, Wang MR, Yuan Y, et al. SD-OCT with prolonged scan depth for imaging the anterior segment of the eye. *Ophthalmic Surg Lasers Imaging* 2010;41(suppl):S65–S69.
56. Yadav R, Ahmad K, Yoon G. Scanning system design for large scan depth anterior segment optical coherence tomography. *Opt Lett*. 2010;35:1774–1776.
57. Birkenfeld J, de Castro A, Marcos S. Contribution of shape and gradient refractive index to the spherical aberration of isolated human lenses. *Invest Ophthalmol Vis Sci*. 2014;55:2599–2607.
58. Birkenfeld J, de Castro A, Marcos S. Astigmatism of the ex vivo human lens: surface and gradient refractive index age-dependent contributions. *Invest Ophthalmol Vis Sci*. 2015; 56:5067–5073.
59. Grulkowski I, Gora M, Szkulmowski M, et al. Anterior segment imaging with Spectral OCT system using a high-speed CMOS camera. *Opt Express*. 2009;17:4842–4858.
60. Marcos S, Ortiz S, Perez-Merino P, Birkenfeld J, Duran S, Jimenez-Alfaro I. Three-dimensional evaluation of accommodating intraocular lens shift and alignment in vivo. *Ophthalmology*. 2014;121:45–55.
61. de Castro A, Ortiz S, Gambra E, Siedlecki D, Marcos S. Three-dimensional reconstruction of the crystalline lens gradient index distribution from OCT imaging. *Opt Express*. 2010;18: 21905–21917.
62. Borja D, Siedlecki D, de Castro A, et al. Distortions of the posterior surface in optical coherence tomography images of the isolated crystalline lens: effect of the lens index gradient. *Biomed Opt Express*. 2010;1:1331–1340.
63. Ortiz S, Siedlecki D, Perez-Merino P, et al. Corneal topography from spectral optical coherence tomography (sOCT). *Biomed Opt Express*. 2011;2:3232–3247.
64. Drexler W, Baumgartner A, Findl O, Hitzenberger CK, Sattmann H, Fercher AF. Submicrometer precision biometry of the anterior segment of the human eye. *Invest Ophthalmol Vis Sci*. 1997;38:1304–1313.
65. Navarro R, Gonzalez L, Hernandez JL. Optics of the average normal cornea from general and canonical representations of its surface topography. *J Opt Soc Am A Opt Image Sci Vis*. 2006;23:219–232.
66. Gerometta R, Zamudio AC, Escobar DP, Candia OA. Volume change of the ocular lens during accommodation. *Am J Physiol Cell Physiol*. 2007;293:C797–804.
67. Lister LJ, Suheimat M, Verkicharla PK, Mallen EAH, Atchison DA. Influence of gravity on ocular lens positioninfluence of gravity on ocular lens position. *Invest Ophthalmol Vis Sci*. 2016;57:1885–1891.
68. Rosales P, Marcos S. Pentacam Scheimpflug quantitative imaging of the crystalline lens and intraocular lens. *J Refract Surg*. 2009;25:421–428.
69. Siedlecki D, de Castro A, Gambra E, et al. Distortion correction of OCT images of the crystalline lens: gradient index approach. *Optom Vis Sci*. 2012;89:E709–E718.

Investigative Ophthalmology & Visual Science